Plant Communications, Volume *4*

Supplemental information

Subfunctionalization of a monolignol to a phytoalexin glucosyltransferase is accompanied by substrate inhibition

Jieren Liao, Guangxin Sun, Elisabeth Kurze, Wieland Steinchen, Timothy D. Hoffmann, Chuankui Song, Zhiwei Zou, Thomas Hoffmann, and Wilfried G. Schwab

SUPPLEMENTAL MATERIAL

Subfunctionalization of a monolignol to a phytoalexin glucosyltransferase is accompanied by substrate inhibition

Jieren Liao[1#], Guangxin Sun[1#, a], Elisabeth Kurze[1#], Wieland Steinchen[2], Timothy D. Hoffmann[1], Chuankui Song[3], Thomas Hoffmann[1], Wilfried G. Schwab[1*]

[1]Biotechnology of Natural Products, Technische Universität München, Liesel-Beckmann-Str. 1, 85354 Freising, Germany

[2]Center for Synthetic Microbiology (SYNMIKRO) & Faculty of Chemistry, Philipps-University Marburg, Karl-von-Frisch-Straße 14, 35043 Marburg, Germany

[3]State Key Laboratory of Tea Plant Biology and Utilization, International Joint Laboratory on Tea Chemistry and Health Effects, Anhui Agricultural University, 230036 Hefei, Anhui, P. R. China

Present address:

[a] Department of Molecular Biophysics and Biochemistry, Yale University, New Haven, Connecticut, USA

[#] These authors contributed equally to this work

* Corresponding author

Table S1. Kinetics of NbUGT72AY1 and StUGT72AY2 towards different substrates. Experimental data were determined by UDP-Glo™ Glycosyltransferase assay and fitted to the partial uncompetitive inhibition model (Eq. 4). Complete uncompetitive inhibition is achieved when v_i is 0. The concentration of UDP-Glc in the reactions was kept fixed (100 µM).

	v_{max} (nmol/min/mg)	v_i (nmol/min/mg)	K_m (µM)	K_i (µM)	n	x	R
NbUGT72AY1							
scopoletin	265.6 +/- 23.6	9 +/- 4	3.1 +/- 0.5	4.6 +/- 1.4	2 +/- 0.5	1 +/- 0.1	0.96
umbelliferone	270.9 +/- 17.5	29.2 +/- 4.8	9.4 +/- 0.8	41.2 +/- 7.9	2 +/- 0.3	1 +/- 0.1	0.98
vanillin	243.4 +/- 15.2	12.6 +/- 8.5	15.9 +/- 3	98.8 +/- 25.4	1 +/- 0.2	1 +/- 0.1	0.98
carvacrol	252.4 +/- 23	108.8 +/- 2.2	9.0 +/- 4.2	44.8 +/- 7.2	1 +/- 0.1	2 +/- 0.2	0.99
coniferyl aldehyde	59.2 +/- 4.1	0	76.8 +/- 13.3	1023.3 +/- 105.7	1 +/- 0.1	2 +/- 0.3	0.99
coniferyl alcohol	98.4 +/- 8.3	0	74.4 +/- 14.7	760.6 +/- 75.3	1 +/- 0.1	2 +/- 0.4	0.98
4-coumaryl aldehyde	35.1 +/- 5.9	0	84.8 +/- 31.5	683.9 +/- 124.3	1 +/- 0.2	2 +/- 0.5	0.96
4-coumaryl alcohol	16.7 +/- 0.7	0	0.7 +/- 0.4	1090.8 +/- 132.4	0.5 +/- 0.1	2 +/- 0.6	0.95
sinapyl aldehyde	38.6 +/- 6.1	0	20.4 +/- 12.4	2055.9 +/- 755.7	0.5 +/- 0.1	3 +/- 1.5	0.88
sinapyl alcohol	55 +/- 6.4	0	23.4 +/- 6.9	676.6 +/- 76	1.5 +/- 0.3	4 +/- 0.9	0.97
StUGT72AY2							
scopoletin	13.6 +/- 1.3	8.8 +/- 0.3	18.4 +/- 2.5	294.1 +/- 91.0	0.5 +/- 0.1	2 +/- 0.6	0.99
vanillin*	15.3 +/- 0.6		62.9 +/- 10.6				
carvacrol	28.8 +/- 8.1	0	221.1 +/- 98.4	1277.3 +/- 746.3	1 +/- 0.1	1 +/- 0.3	0.99
coniferyl aldehyde*	21.6 +/- 1.4		145.8 +/- 45.0				
coniferyl alcohol*	18.9 +/- 0.5		62.6 +/- 8.1				0.99
sinapyl aldehyde	42.4 +/- 4	0	18.5 +/- 156.9	1370.2 +/- 0	1 +/- 0.1	2 +/- 0.2	0.99
sinapyl alcohol*	39.4 +/- 2.8		139.6 +/- 29.3				0.99

The abbreviations are v_{max}: the maximal reaction rate; K_m: Michaelis-Menton constant reflecting the substrate concentration at which the reaction rate is half of v_{max}; K_i: the inhibition constant which is the concentration of inhibitor required to decrease the maximal rate of the reaction to half of the uninhibited value; v_i: the reaction velocity in the presence of inhibition; n, x: Hill coefficient; * Substrates marked with an asterisk show Michaelis-Menten kinetics (Equation 1).

Table S3. List of primers

Name	Sequence
NbUGT72AY1-Forward	GAAGATCTATGGATAGCTCACAACTT
NbUGT72AY1-Reverse	CCCTCGAGTTACAACTCTCTGCTCCG
NbUGT72AY1- Mutant I86V;F87I-Forward	TAATAAATTCCAGCACTAAAGTTATCACTCAATTACGACTATTGGT
NbUGT72AY1- Mutant I86V;F87I-Reverse	ACCAATAGTCGTAATTGAGTGATAACTTTAGTGCTGGAATTTATTA
NbUGT72AY1- Mutant H390Y –Forward	TTGCATGGCCATTATACGCTGAACAAAAAATG
NbUGT72AY1- Mutant H390Y – Reverse	CATTTTTTGTTCAGCGTATAATGGCCATGCAA
NbUGT72AY1 Chimeric N Term Forward	CCCCCGGGTATGGATAGCTCACAACTT
NbUGT72AY1 Chimeric C Term Reverse	CCCTCGAGTTACAACTCTCTGCTCCG
NbUGT72AY1 Chimeric Start Forward	GCTATATATTGTCAAGTTATCGACCAAGAG
NbUGT72AY1 Chimeric Start Reverse	CTCTTGGTCGATAACTTGACAATATATAGC
NbUGT72AY1 Chimeric End Forward	GTACACGTGCTTCGATGGAATATTGATTAA
NbUGT72AY1 Chimeric End Reverse	TTAATCAATATTCCATCGAAGCACGTGTAC
NbUGT72AY1- Mutant N27D -Forward	CTAGTCTTAGGCGACCGATTAGCCACT
NbUGT72AY1- Mutant N27D - Reverse	AGTGGCTAATCGGTCGCCTAAGACTAG
StUGT72AY2- Mutant I86V;F87I -Forward	GACAGTACGACCAAGATCTTCACGCAACTGCGTCTG
StUGT72AY2- Mutant I86V;F87I -Reverse	CAGACGCAGTTGCGTGAAGATCTTGGTCGTACTGTC
StUGT72AY2- Mutant H390Y –Forward	ATCGCGTGGCCGCTGCACGCGGAACAGAAGATGAAT
StUGT72AY2- Mutant H390Y - Reverse	ATTCATCTTCTGTTCCGCGTGCAGCGGCCACGCGAT
StUGT72AY2 Chimeric N Term Forward	CGGAATTCATGGATAATACCCAGCTCCA
StUGT72AY2 Chimeric C Term Reverse	ATTTGCGGCCGCTTAGCGCGTGCGGATATCC
StUGT72AY2 Chimeric Start Forward	TTTATCTACCAGCAAGTTTTCGACAAAGAA
StUGT72AY2 Chimeric Start Reverse	TTCTTTGTCGAAAACTTGCTGGTAGATAAA
StUGT72AY2 Chimeric End Forward	TACAGATTTTGATGGTATCCTCATCAACAC
StUGT72AY2 Chimeric End Reverse	GTGTTGATGAGGATACCATCAAAATCTGTA
StUGT72AY2- Mutant N27D -Forward	CCAGTGCTGGTGCTGGGTGACCGCCTCGCGACCAAC
StUGT72AY2- Mutant N27D - Reverse	GTTGGTCGCGAGGCGGTCACCCAGCACCAGCACTGG
NbUGT72AY1- Mutant R91A - Forward	AAATTTTCACTCAATTAGCACTATTGGTCCGTGAAG
NbUGT72AY1- Mutant R91A - Reverse	CTTCACGGACCAATAGTGCTAATTGAGTGAAAATTT
NbUGT72AY1- Mutant R91M - Forward	AAATTTTCACTCAATTAATGCTATTGGTCCGTGAAG
NbUGT72AY1- Mutant R91M - Reverse	CTTCACGGACCAATAGCATTAATTGAGTGAAAATTT
NbUGT72AY1- Mutant R91F - Forward	AAATTTTCACTCAATTATTCCTATTGGTCCGTGAAG
NbUGT72AY1- Mutant R91F - Reverse	CTTCACGGACCAATAGGAATAATTGAGTGAAAATTT
NbUGT72AY1- Mutant I86V - Forward	TAAATTCCAGCACTAAAGTTTTCACTCAATTACGACTATT
NbUGT72AY1- Mutant I86V - Reverse	AATAGTCGTAATTGAGTGAAAACTTTAGTGCTGGAATTTA
NbUGT72AY1- Mutant F87I - Forward	TAAATTCCAGCACTAAAATTATCACTCAATTACGACTATT
NbUGT72AY1- Mutant F87I - Reverse	AATAGTCGTAATTGAGTGATAATTTTAGTGCTGGAATTTA

Table S4. Diagnostic ions and ion traces for the detection of products by LC-MS.

Products	Diagnostic ions for detection of the products	Ion trace (*m/z*)	Retention time (min)
Scopoletin glucoside	$[M+Cl]^-$	389	9.1
	$[M+HCOO]^-$	399	
Carvacrol glucoside	$[M+Na]^+$	335	11.0
Sinapyl aldehyde glucoside	$[M+Cl]^-$	405	9.4
	$[M+HCOO]^-$	415	
Sinapyl alcohol 4-*O*-glucoside	$[M+Cl]^-$	407	21.9
	$[M+HCOO]^-$	417	
Sinapyl alcohol 1-*O*-glucoside	$[M+Cl]^-$	407	23.3
	$[M+HCOO]^-$	417	
Coniferyl aldehyde glucoside	$[M+Cl]^-$	377	9.1
	$[M+HCOO]^-$	387	
Coniferyl alcohol 4-*O*-glucoside	$[M+Cl]^-$	377	20.0
	$[M+HCOO]^-$	387	
Coniferyl alcohol 1-*O*-glucoside	$[M+Cl]^-$	377	23.7
	$[M+HCOO]^-$	387	

NbUGT72AY1 expression data

StUGT72AY2 expression data

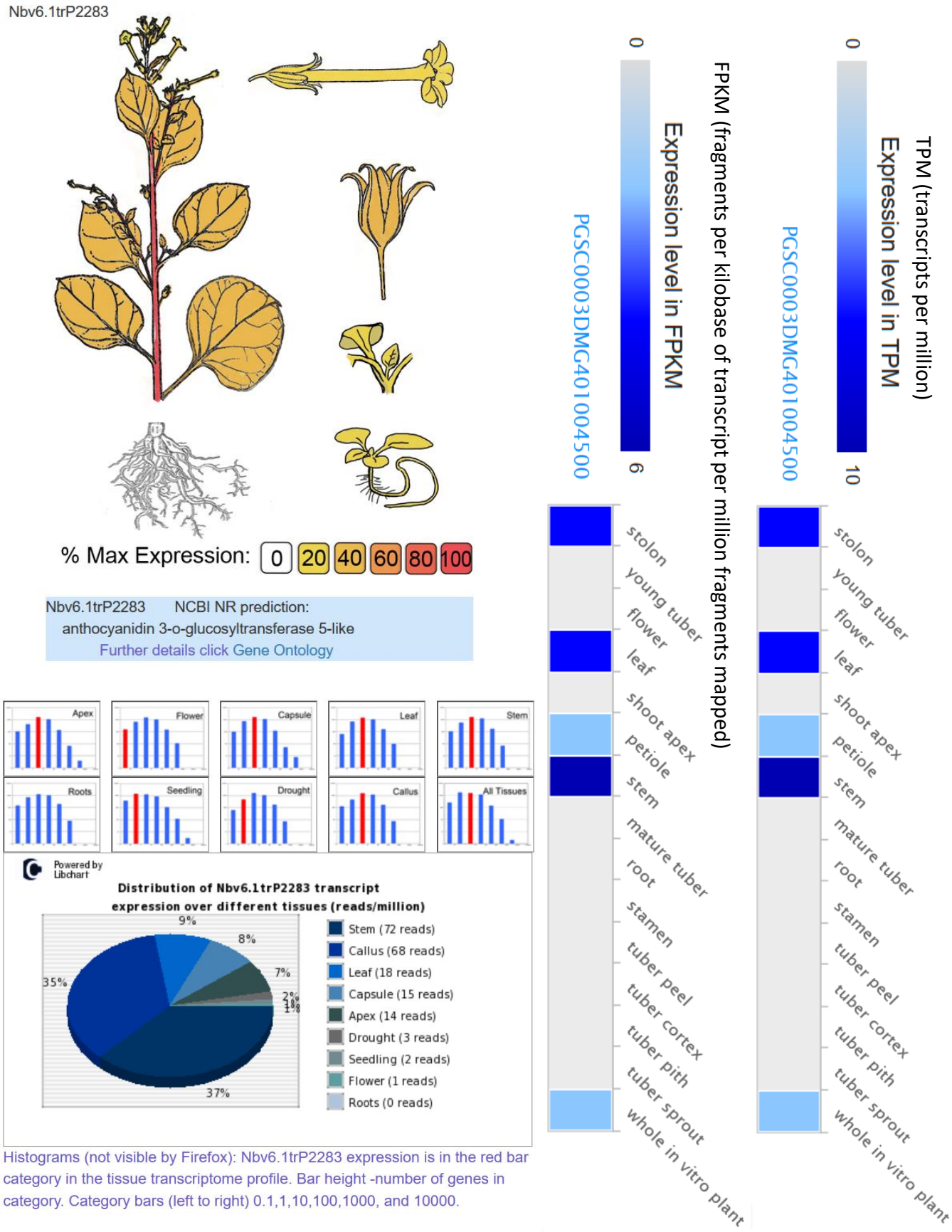

Fig. S1 NbUGT72AY1 and StUGT72AY2 expression data retrieved from https://sefapps02.qut.edu.au/atlas/tREXXX2new6.php?TrID=Nbv6.1trP2283; (December 20, 2021) and www.ebi.ac.uk/gxa/experiments/E-MTAB-552/; accession PGSC0003DMG401004500; (December 20, 2021), respectively.

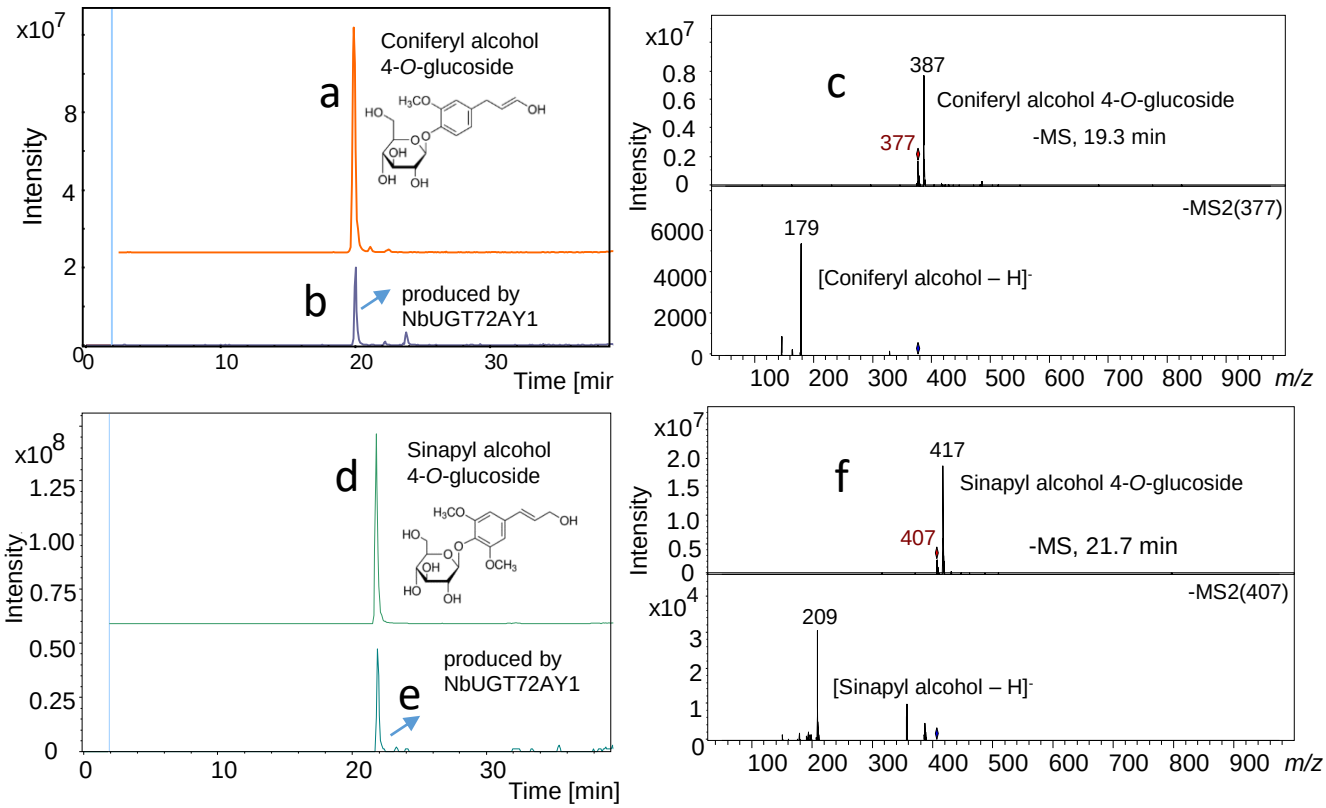

Fig. S2. LC-MS analysis of reference material and products formed after the incubation of coniferyl alcohol and sinapyl alcohol with NbUGT72AY1. **a** Reference coniferyl alcohol 4-*O*-glucoside. **b** enzymatic product. **c** MS and MS2 of the product. **d** Reference sinapyl alcohol 4-*O*-glucoside. **e** enzymatic product. **f** MS and MS2 of the product.

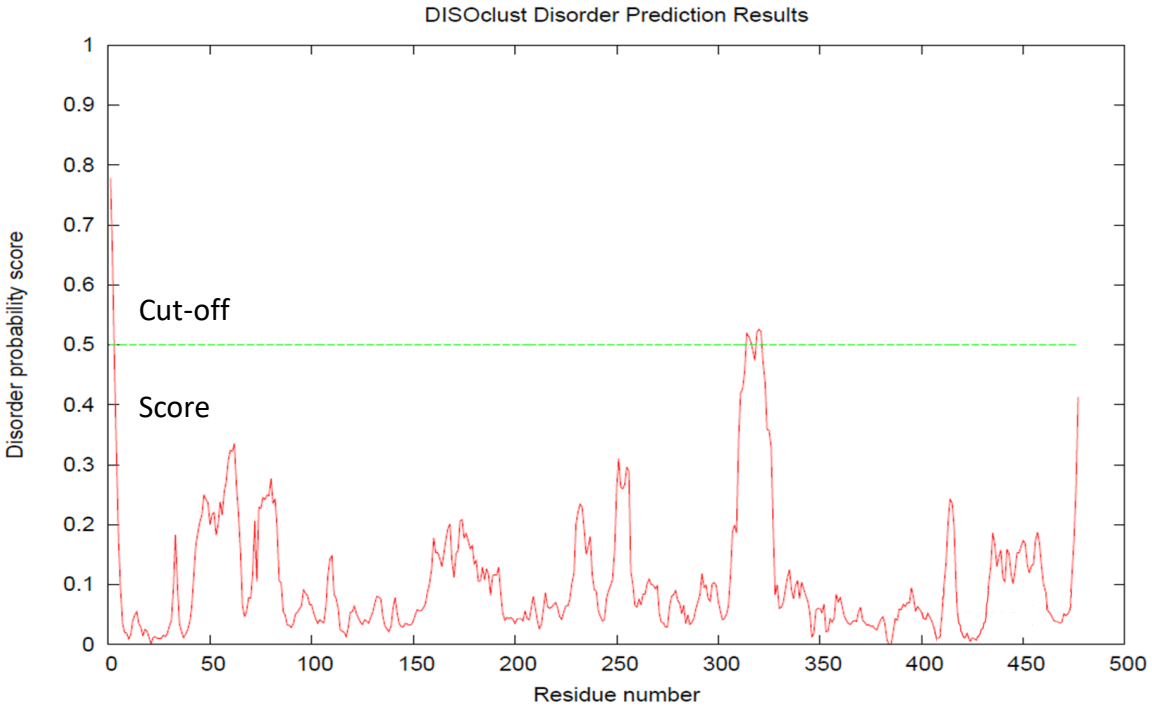

Fig. S3. Disorder prediction graph for the 3D model of NbUGT72AY1. Calculated by the IntFOLD server according to (McGuffin et al., 2019). Cut-off value (green line) and score of individual amino acids (red line) are shown.

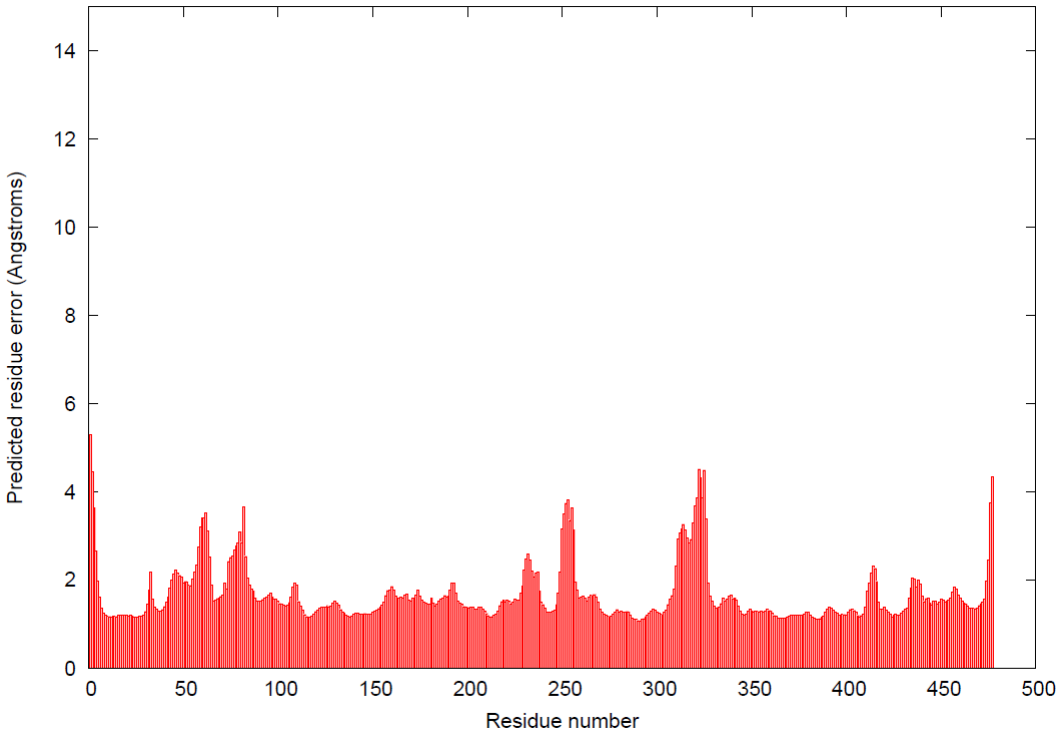

Fig. S4. Local NbUGT72AY1 model quality plot calculated by the IntFOLD server (McGuffin et al., 2021).

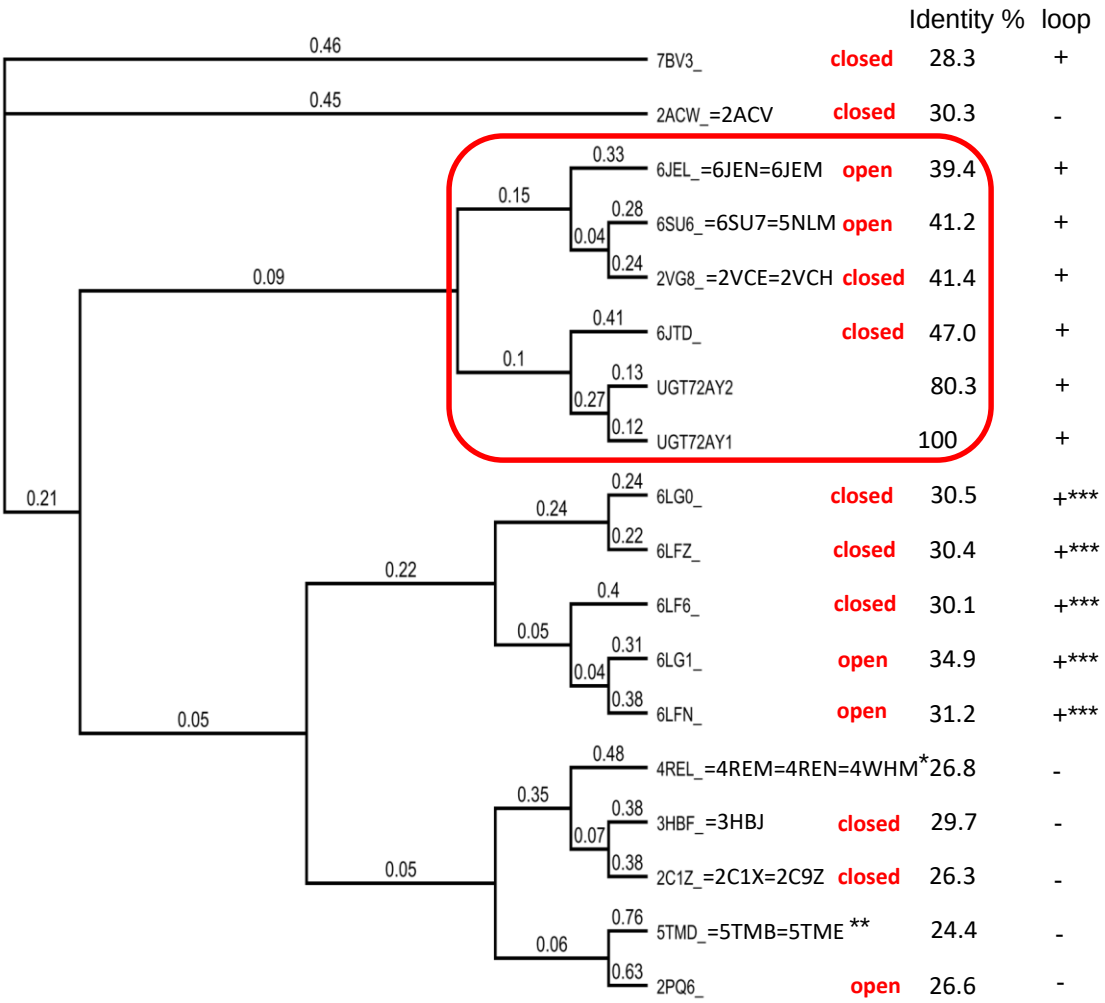

Fig S5. Phylogentic tree of family 1 glycosyltransferases (GT1) according to the CAZy database (www.cazy.org/GlycosylTransferases.html) whose 3D stuctures have been elucidated. The tree shows the accession numbers of the Protein Data Bank (www.rcsb.org) and their amino acid sequence identities with NbUGT72AY1. The decision of closed and open conformer was based on the orientation of the first amino acid Trp of the PSPG box. * open and closed conformers were found. Trp appears to rotate during soaking. ** Trp is replaced by Phe. Two different alignments of Phe are discernible. Structures containing a similar flexible loop (aa 312-330) as in 6JTD are marked in the last column. *** The loop contains about 10 amino acids less than the proteins at the top.

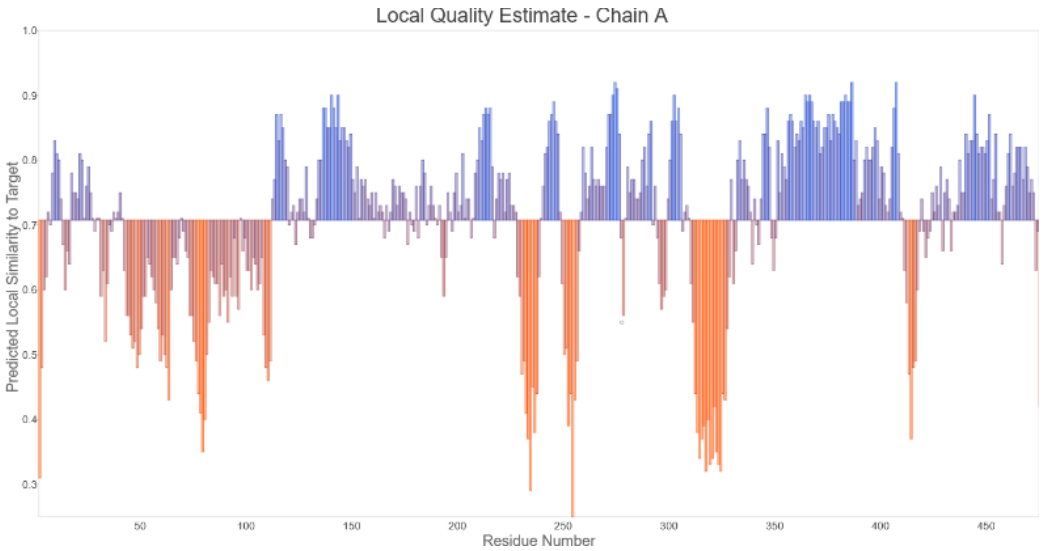

Fig. S6. Local quality estimate of the 3D model of NbUGT72AY1 (open conformer) calculated by the SWISS MODEL server according to (Waterhouse et al., 2018).

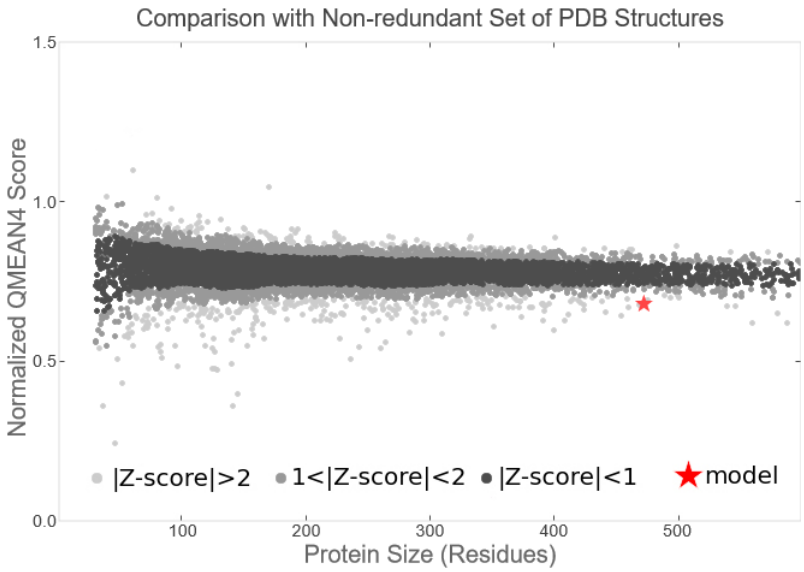

Fig. S7. Quality assessment of the 3D model of NbUGT72AY1 (open conformer) calculated by the SWISS MODEL server according to (Waterhouse et al., 2018).

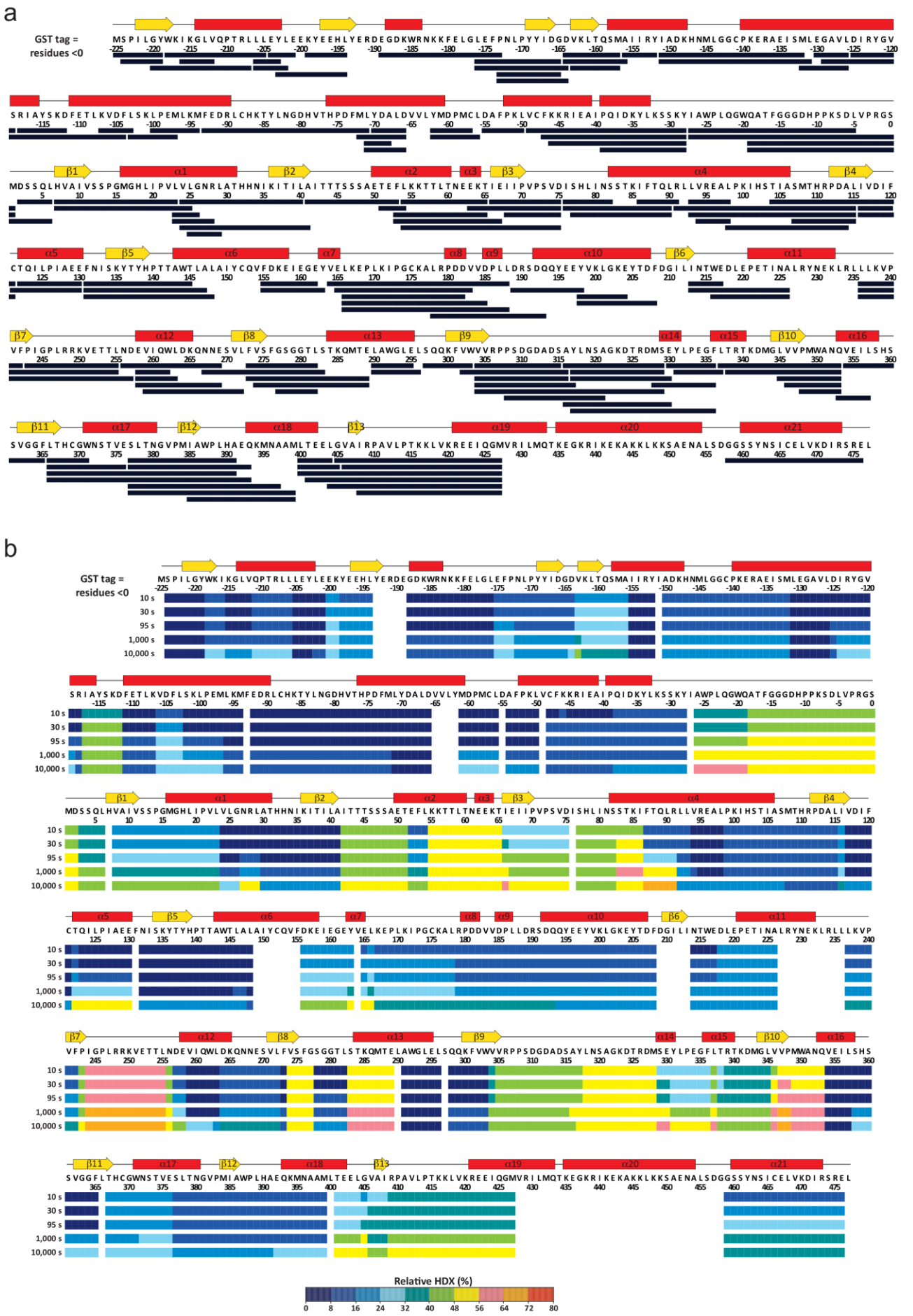

Fig. S8. HDX-MS of NbUGT72AY1. a NbUGT72AY1peptides (peptide coverage map) analysed by HDX-MS. Each black bar represents a peptide that was evaluated for D-incorporation. Amino acids with numbers <0 are part of the GST tag. **b** HDX of apo-NbUGT72AY1. The predicted secondary structure is indicated above the amino acid sequences (red, α-helix; yellow, β-strand). Relative deuterium uptake of NbUGT72AY1 after different time intervals. D-incorporation NbUGT72AY1 colored in rainbow from blue (0 %) to red (100% D-incorporation).

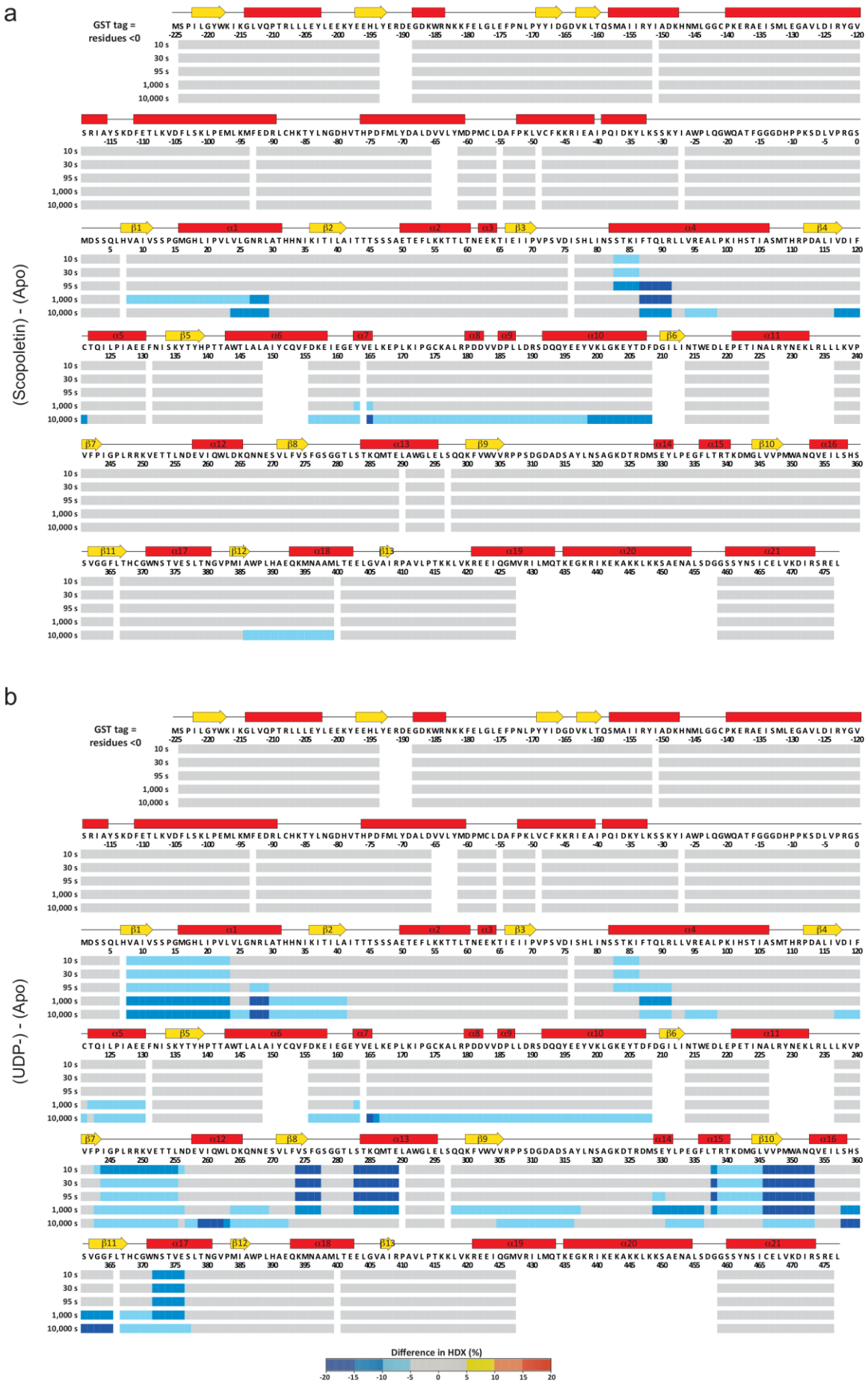

Fig. S9. Conformational changes of NbUGT72AY1 related to substrate binding. a Differences in deuterium uptake between scopoletin-bound and apo-NbUGT72AY1. **b** Differences in deuterium uptake between UDP-bound and apo-NbUGT72AY1. Differences are displayed on the amino acid sequence of the protein. The predicted secondary structure is indicated above (red, α-helix; yellow, β-strand). Blue boxes show regions with less HDX in the presence of scopoletin or UDP. Regions with increased HDX in the presence of scopoletin or UDP were not observed.

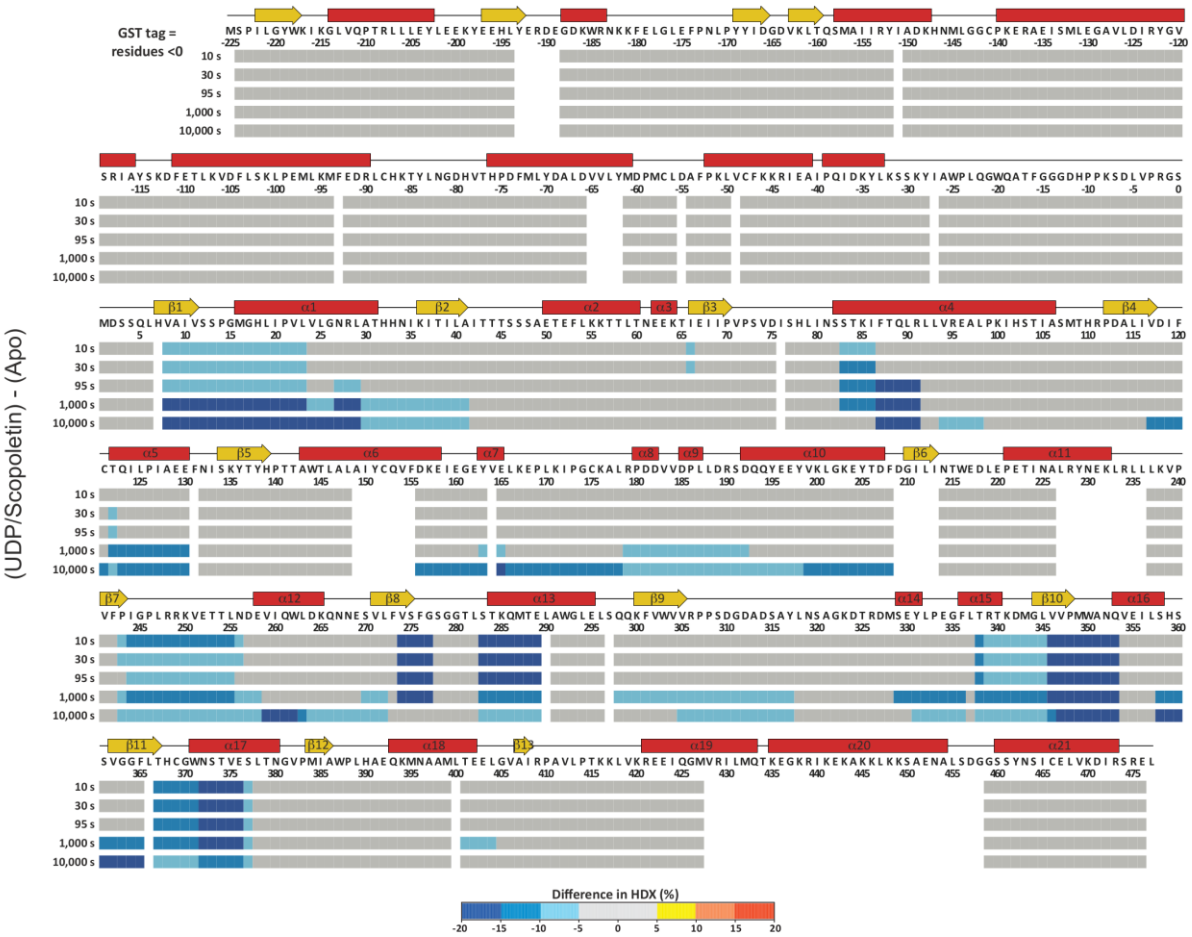

Fig. S10. Conformational changes of NbUGT72AY1 related to scopoletin/UDP binding. Difference in deuterium uptake between scopoletin-/UDP-bound and apo-NbUGT72AY1. Differences are displayed on the amino acid sequence of the protein. The predicted secondary structure is indicated above (red, α-helix; yellow, β-strand). Blue boxes show regions with less HDX in the presence of scopoletin or UDP. Regions with increased HDX in the presence of scopoletin/UDP were not observed.

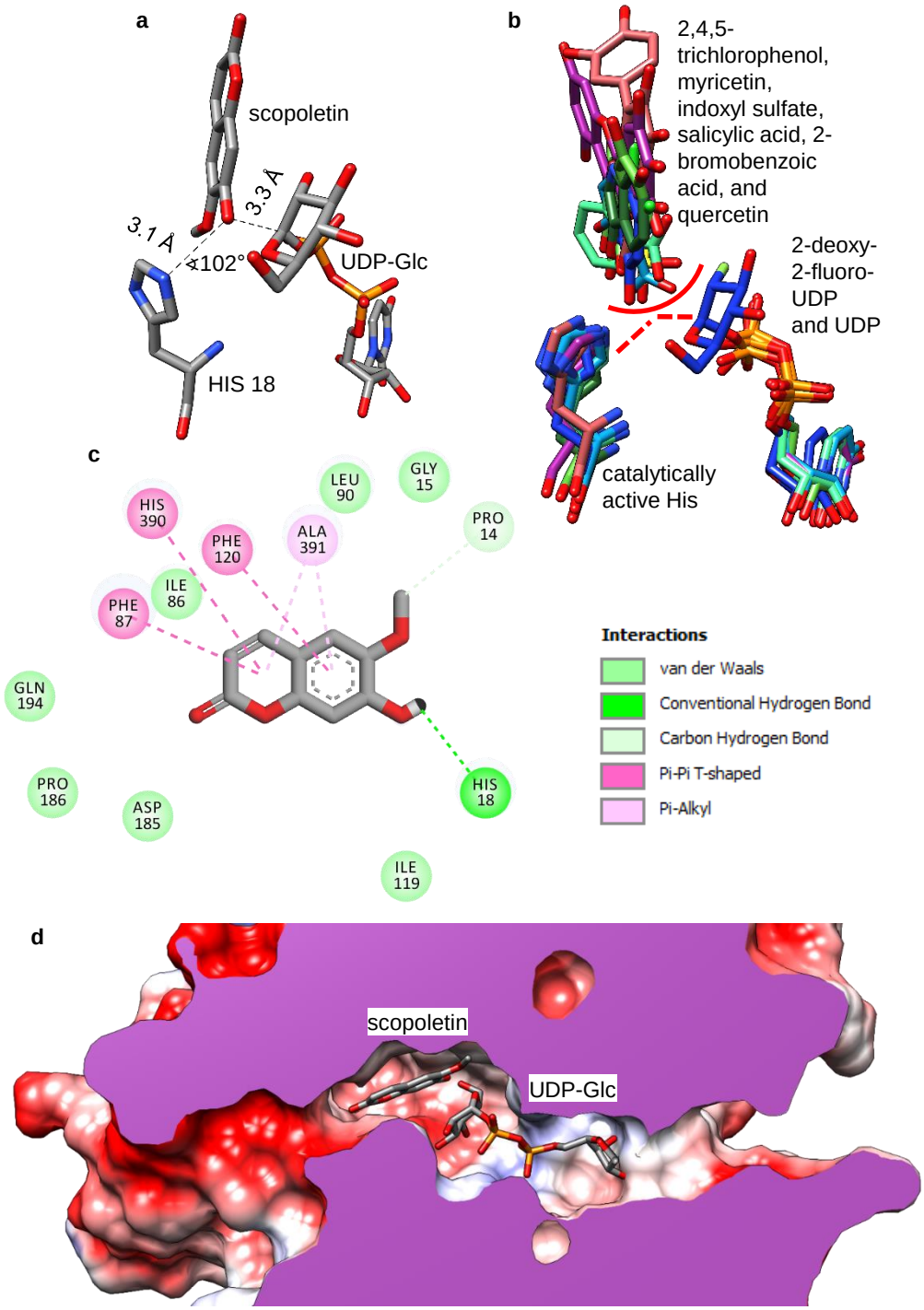

Fig S11. Scopoletin docking in NbUGT72AY1. a Ligand docking was performed with the Autodock/Vina tool (http://vina.scripps.edu/download.html) implemented into UCSF Chimera 1.15 (https://www.cgl.ucsf.edu/chimera/download.html) using default values. Structure 2VCE was used as template for positioning of scopoletin. **b** Superimposition of UGT structures showing their substrates/substrate analogs and the catalytically active His. The following 3D protein structures were used; 2VCE (2-deoxy-2-fluoro-UDP and 2,4,5-trichlorophenol), 3HBF (myricetin and UDP), 5NLM (indoxyl sulfate), 5U6M (salicylic acid and UDP), 5V2K (2-bromobenzoic acid and UDP), 6IJD (quercetin), and 2C9Z (quercetin and UDP). Please note that the imidazole ring of the catalytically active His is rotated by 50° in structures where glucose or a glucose analog is missing in the complex (2VCE in comparison to the other structures). Since the 3D model of NbUGT72AY1 was predicted based on 6JTD (complex with UDP-Glc), the imidazole ring of His shows the same orientation as in 2VCE. **c** Ligand–protein interactions (scopoletin in the catalytic center) predicted by Discovery Studio Visualizer v19.1.0.18287 (https://discover.3ds.com/discovery-studiovisualizer-Download). **d** Substrate tunnel in the NbUGT72AY1 3D structure. Electrostatic surface potentials are colored red and blue for negative and positive charges, respectively, and white color represents neutral residues.

a

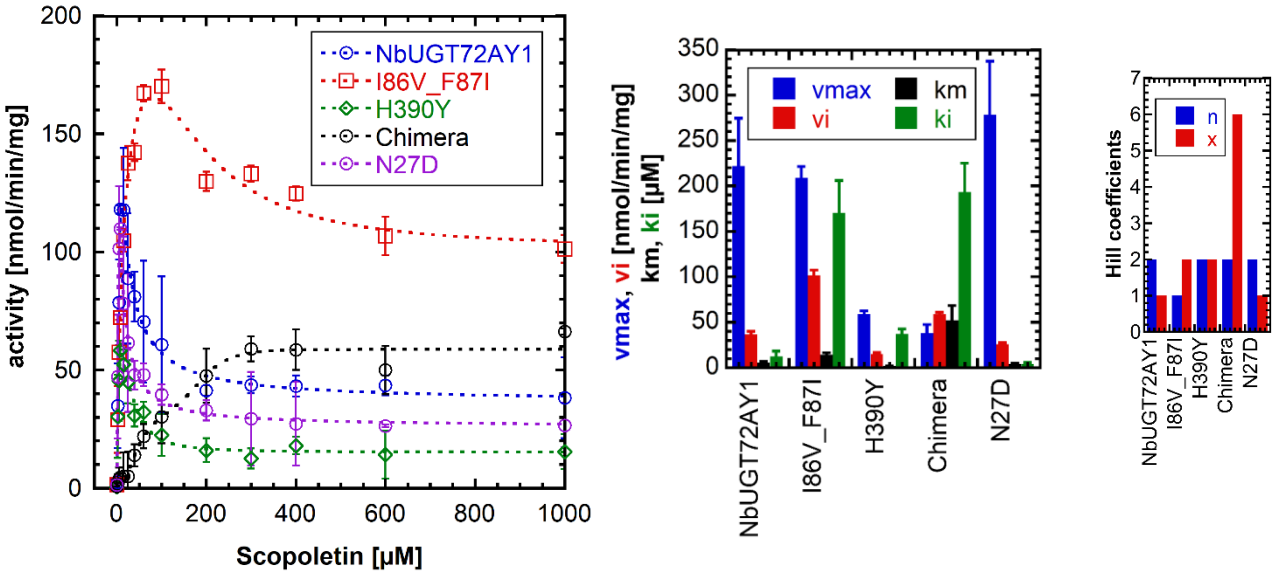

b

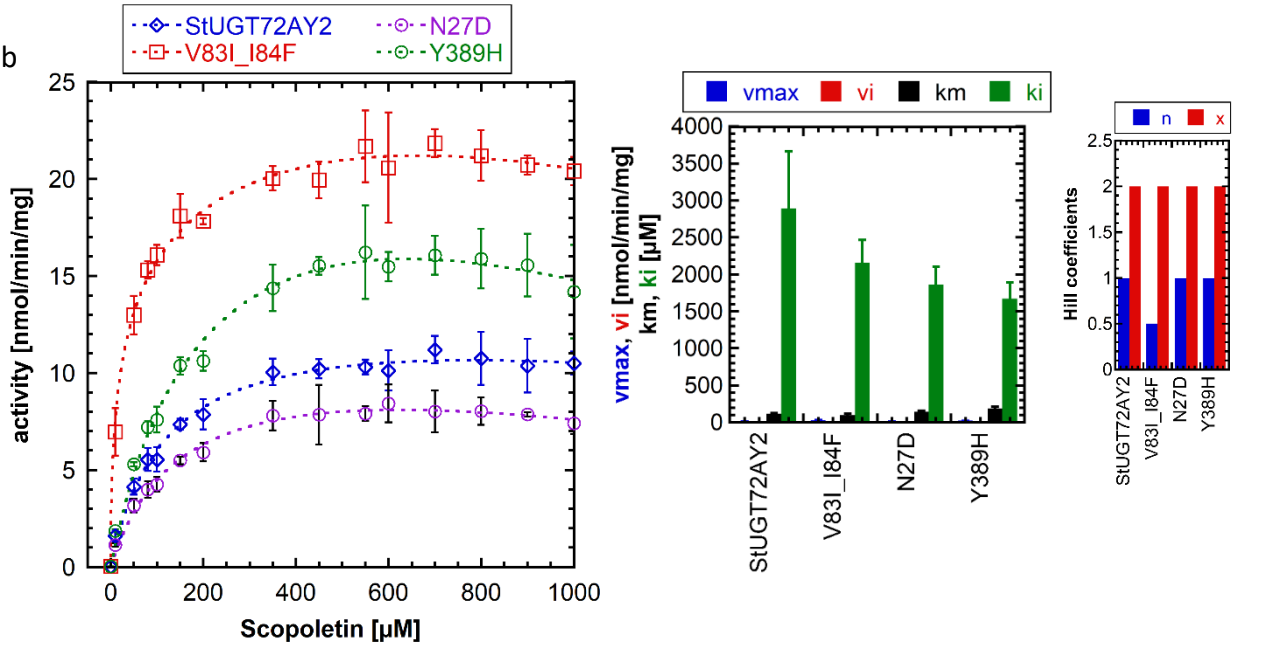

Fig. S12. Kinetic parameters (based on LC-MS data) of NbUGT72AY1, StUGT72AY2, and mutant enzymes using scopoletin as substrates. **a** NbUGT72AY1 and its mutants were used to glucosylate scopoletin. **b** StUGT72AY2 and its mutants were used to glucosylate scopoletin

NbUGT72AY1 https://www.ebi.ac.uk/thornton-srv/databases/pdbsum/Generate.html

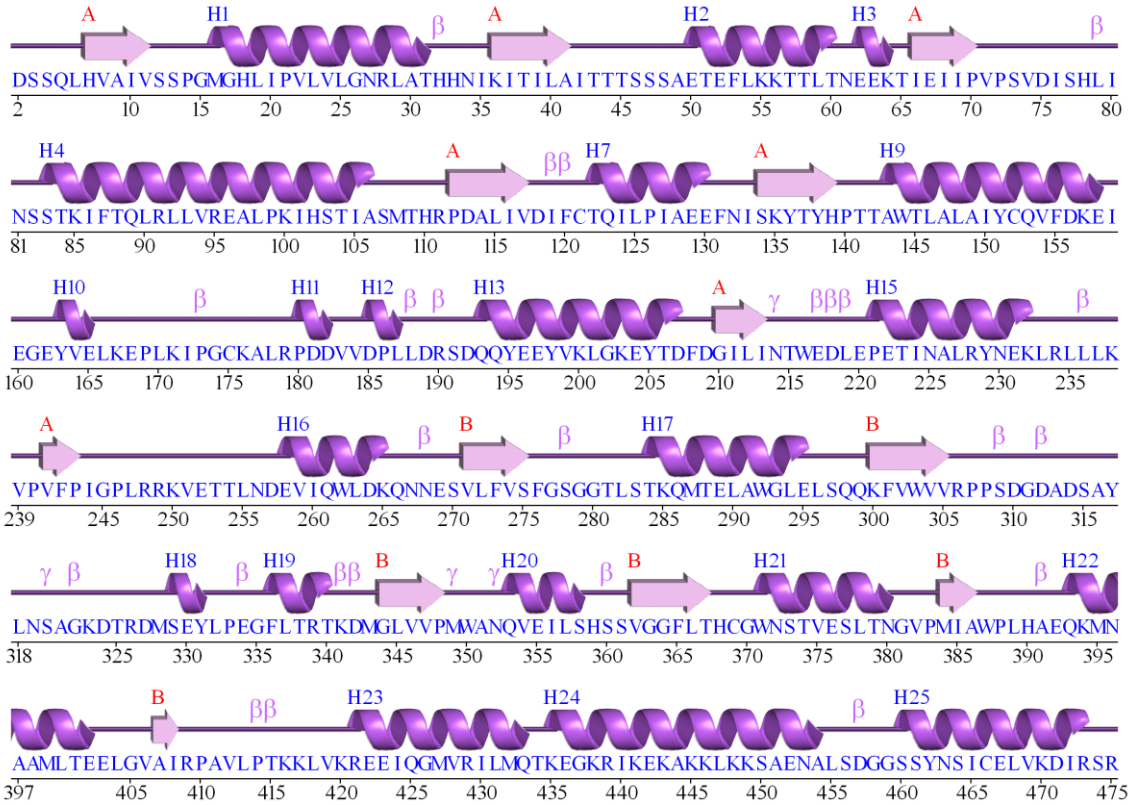

StUGT72AY2 https://www.ebi.ac.uk/thornton-srv/databases/pdbsum/Generate.html

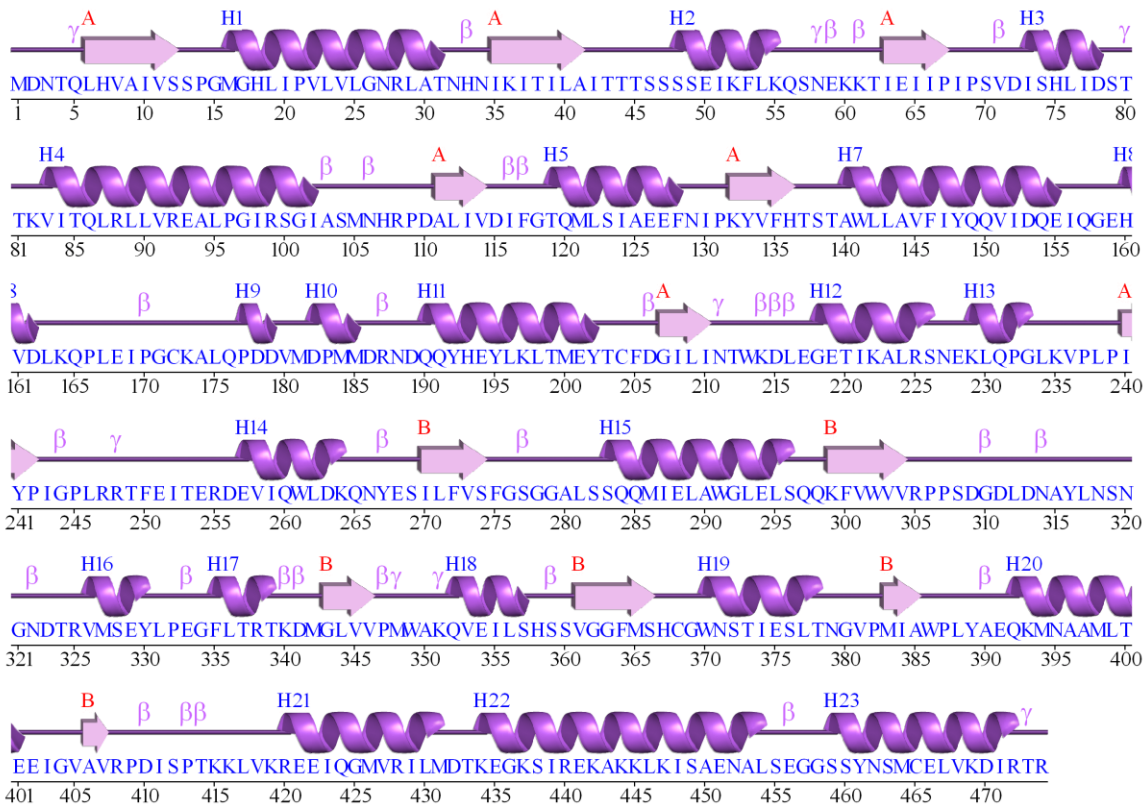

Fig. S13. Predicted secondary structures of NbUGT72AY1 and StUGT72AY2. The wiring diagram is a schematic diagram showing the protein's secondary structure elements (α-helices and β-sheets) together with various structural motifs such as beta- and gamma-turns, and beta-hairpins. Helices are labelled H1, H2, etc while strands are labelled A, B, C, etc according to the beta sheet to which they belong.

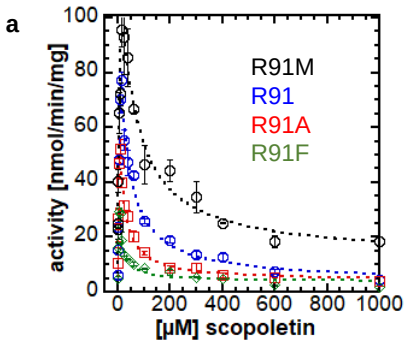

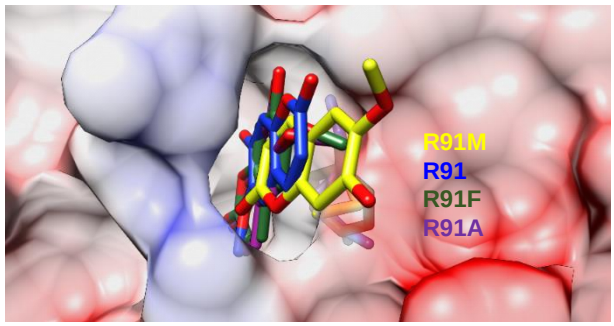

b

mutant	V_{max}	V_i	K_m	K_i	n	x	R
R91	212.0 +/- 8.4	4.4 +/- 2.3	10.8 +/- 1.9	10.7 +/- 2.2	1 +/- 0.2	1 +/- 0.1	0.99
R91A	201.9 +/- 17.3	4.5 +/- 2.0	11.9 +/- 3.0	3.3 +/- 0.7	1 +/- 0.3	1 +/- 0.2	0.97
R91F	222.9+/- 15.1	4.2 +/- 0.8	12.6 +/- 4.7	0.9 +/- 0.3	1 +/- 0.1	1 +/- 0.1	0.98
R91M	196.0 +/- 18.3	13.1 +/- 6.1	10.9 +/- 1.7	27.3 +/- 4.2	1 +/- 0.1	1 +/- 0.1	0.95

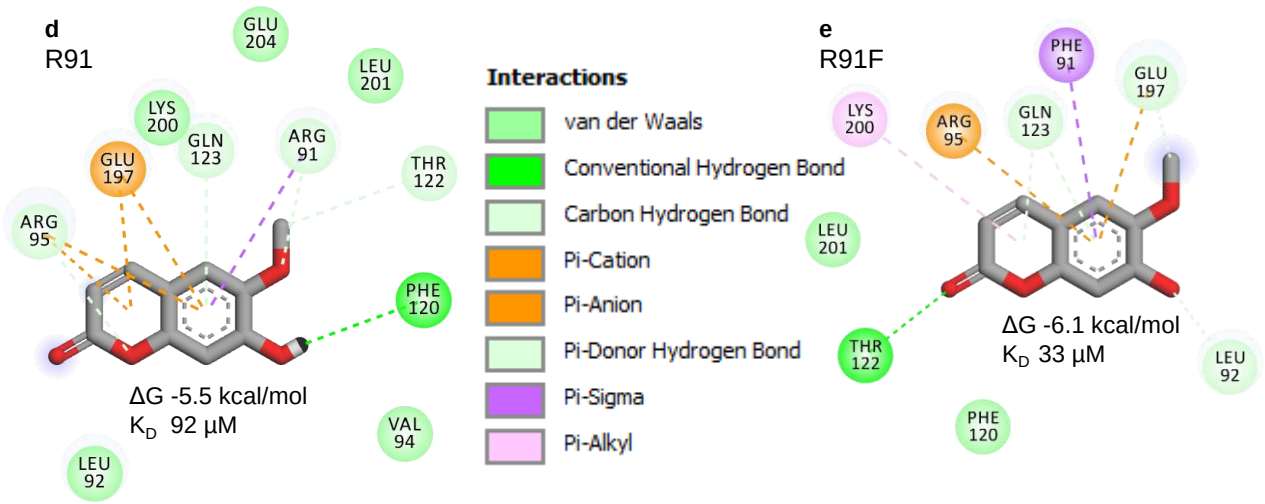

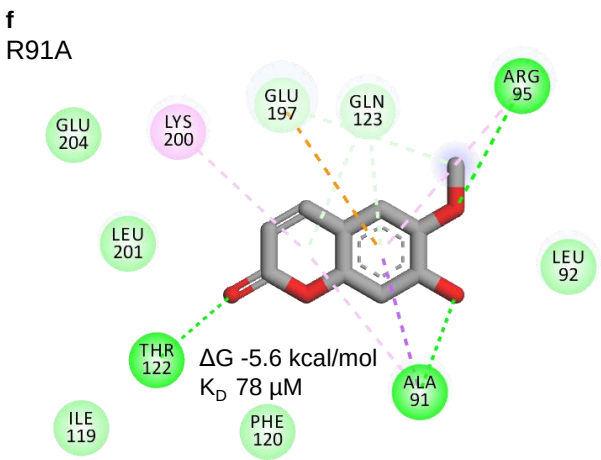

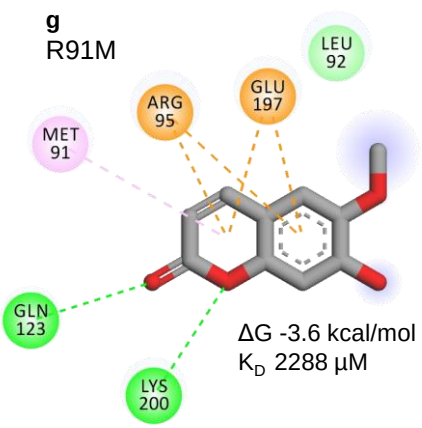

Fig S14. Mutational analysis of R91 demonstrates its involvement in substrate inhibition of NbUGT72AY1. a Two dimensional plots of acceptor substrate concentration versus reaction rate for the wild type enzyme NbUGT72AY1 (R91) and mutants R91A, R91F and R91M. **b** Kinetics of mutants towards scopoletin. **c** Docking of scopoletin into the putative allosteric site of the mutants was performed with the Autodock/Vina tool (http://vina.scripps.edu/download.html) implemented into UCSF Chimera 1.15 (https://www.cgl.ucsf.edu/chimera/download.html) using default values. **d** *In silico* calculated binding energies ΔG (Autodock/Vina) were used to calculate equilibrium constants K_D. The models were visualized by Discovery Studio Visualizer v19.1.0.18287 (https://discover.3ds.com/discovery-studiovisualizer-Download); wild type R91. **e** Mutant R91F. **f** Mutant R91A. **g** Mutant R91M.

a

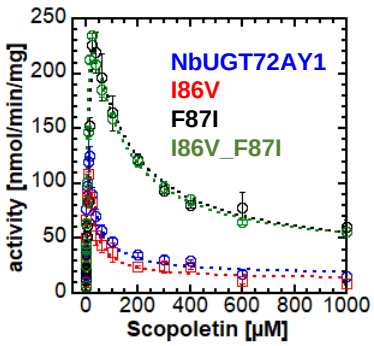

b

mutant	V_{max}	V_i	K_m	K_i	n	x	R
NbUGT72AY1	298.2 +/- 8.4	16.3 +/- 4.0	8.1 +/- 1	11.6 +/- 1.5	1 +/- 0.1	1 +/- 0.1	0.98
I86V	318.9 +/- 10.0	11.6 +/- 3.3	9.8 +/- 1.5	8.6 +/- 1.1	1 +/- 0.1	1 +/- 0.2	0.98
F87I	322 +/- 7.6	29.8 +/- 0.8	13 +/- 4.7	97.4 +/- 0.3	1.5 +/- 0.1	1.1 +/- 0.1	0.98
I86V_F87I	321 +/- 5.8	32 +/- 6.1	8 +/- 1.7	86 +/- 4.2	1.3 +/- 0.1	1 +/- 0.1	0.98

Fig. S15. Mutational analysis to demonstrate the involvement of F87I in substrate inhibition of NbUGT72AY1. a Two dimensional plots of acceptor substrate concentration versus reaction rate for the wild type enzyme NbUGT72AY1 and mutants I86V, F87I, and the double mutant I86V_F87I. **b** Kinetics of mutants towards scopoletin.

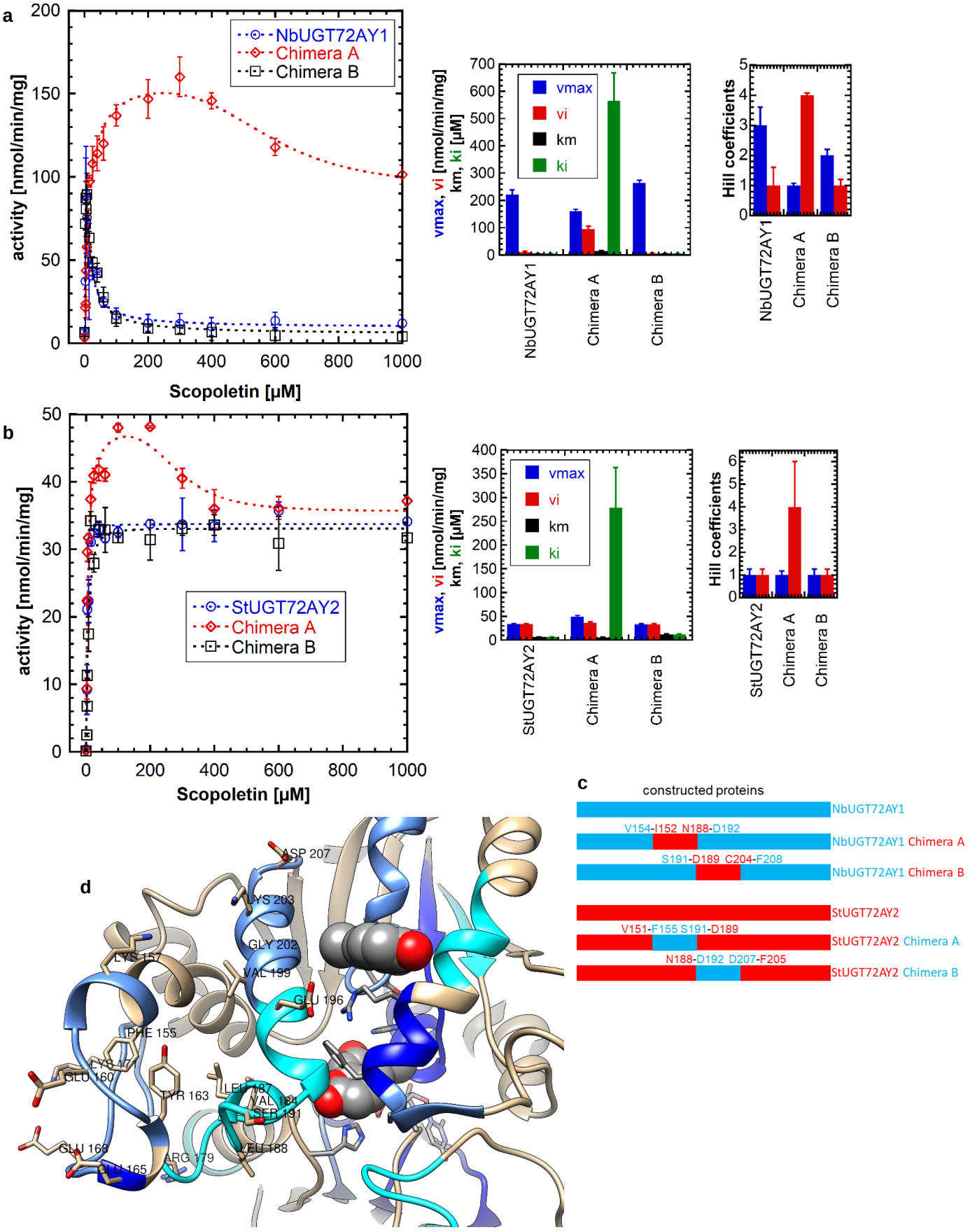

Fig. S16. Kinetic parameters of NbUGT72AY1, StUGT72AY2, and mutant enzymes to identify key amino acids in the chimera sequence responsible for substrate inhibition. Scopoletin was used as substrate. **a** NbUGT72AY1 and its mutants were used to glucosylate scopoletin. **b** StUGT72AY2 and its mutants were used to glucosylate scopoletin. **c** Schemes of the generated mutants. Chimeras A and B contain only part of the original sequence of the chimera mutants. The reciprocal enzymes (StUGT72AY2 versions) were also generated. **d** Predicted NbUGT72AY1 protein model showing the amino acids that differ in the chimeric sequence in NbUGT72AY1 and StUGT72AY2.

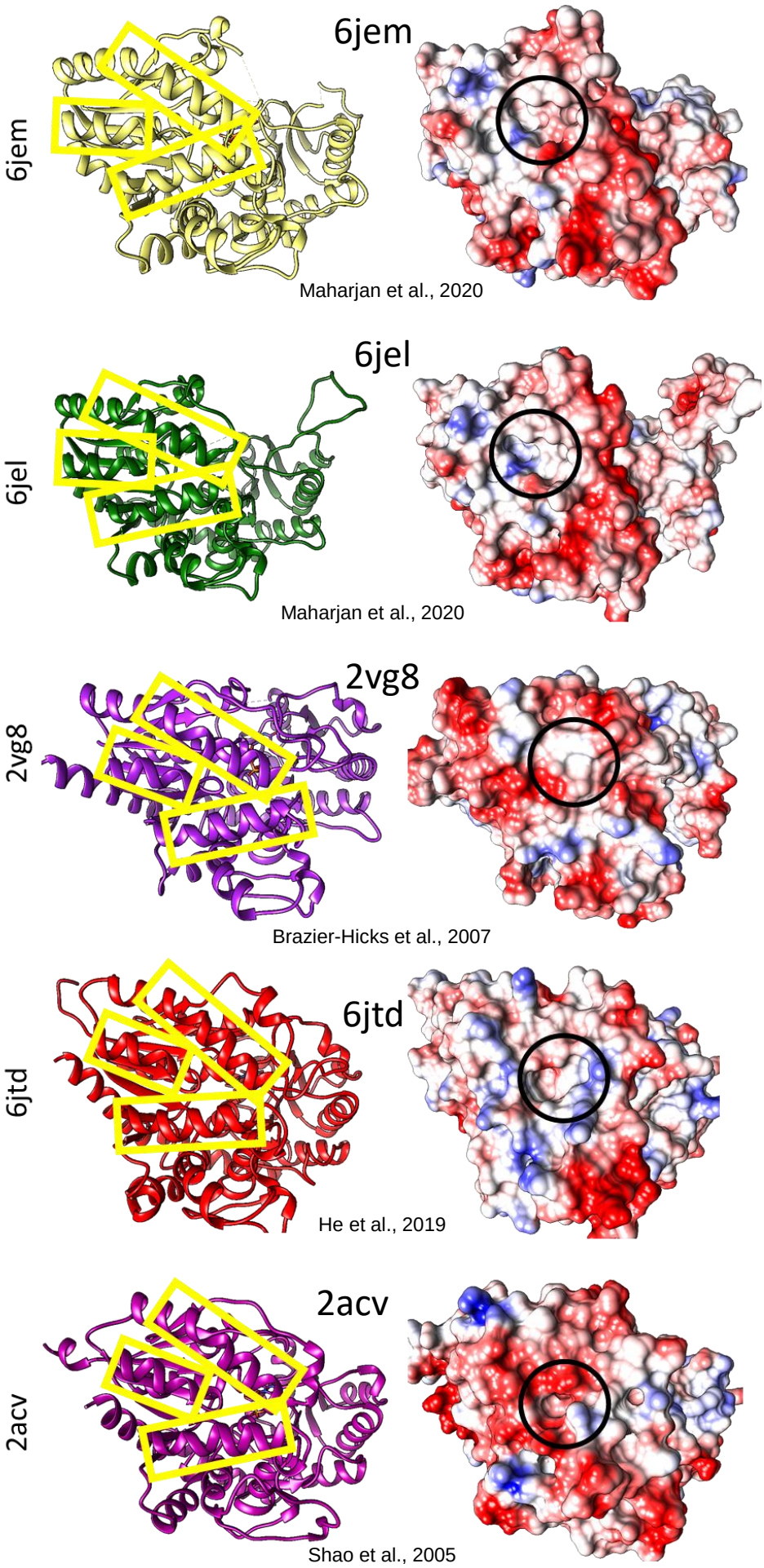

Fig. S17. Putative allosteric site in GT-B-folded UGTs. Structures were uploaded from www.rcsb.org. A black circle indicates the putative allosteric site, which is established by three α-helices (in yellow boxes).

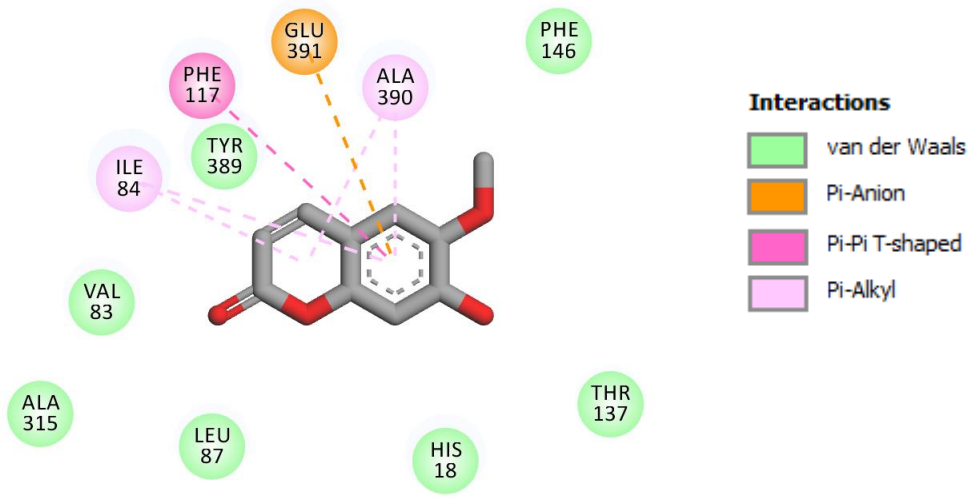

Fig. S18. Docking of scopoletin into the active site of StUGT72AY2. Docking was performed with the Autodock/Vina tool (http://vina.scripps.edu/download.html) implemented into UCSF Chimera 1.15 (https://www.cgl.ucsf.edu/chimera/download.html) using default values.

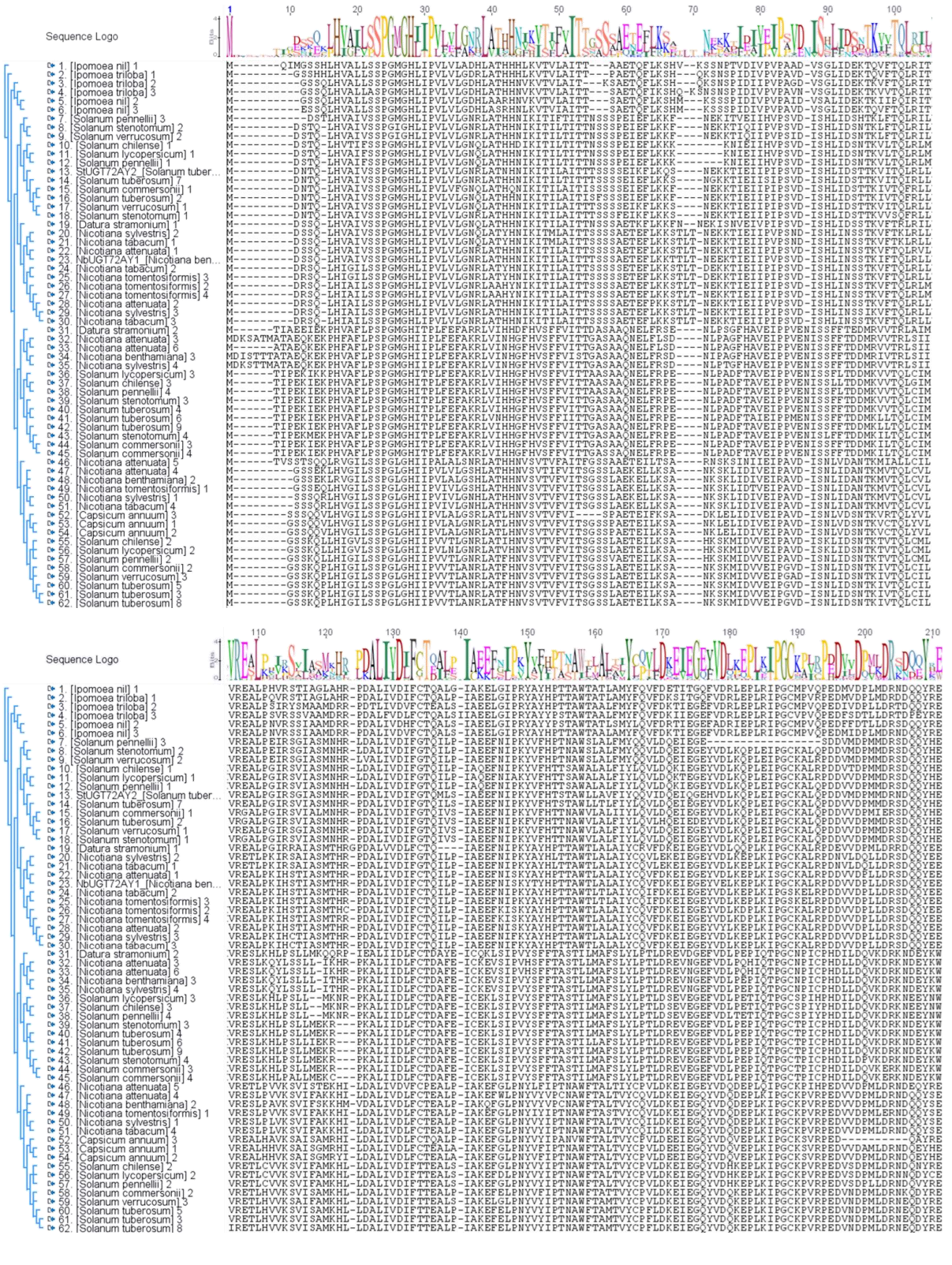

Fig. S19. Phylogenetic analysis of the closed homologues of NbUGT72AY1. The tree shows the protein sequences most similar to NbUGT72AY1 extracted from GenBank (www.ncbi.nlm.nih.gov/genbank/).

Part 1

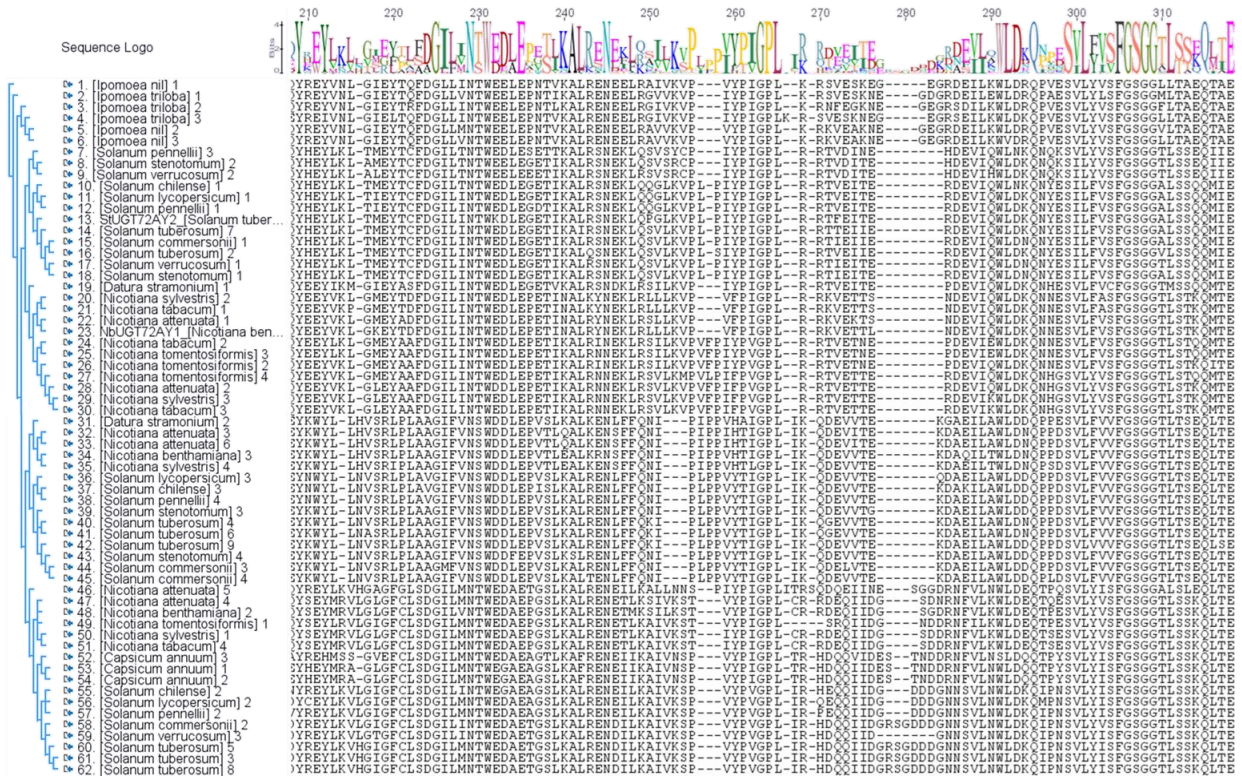

Fig. S19. Phylogenetic analysis of the closed homologues of NbUGT72AY1. The tree shows the protein sequences most similar to NbUGT72AY1 extracted from GenBank (www.ncbi.nlm.nih.gov/genbank/).

Part 2

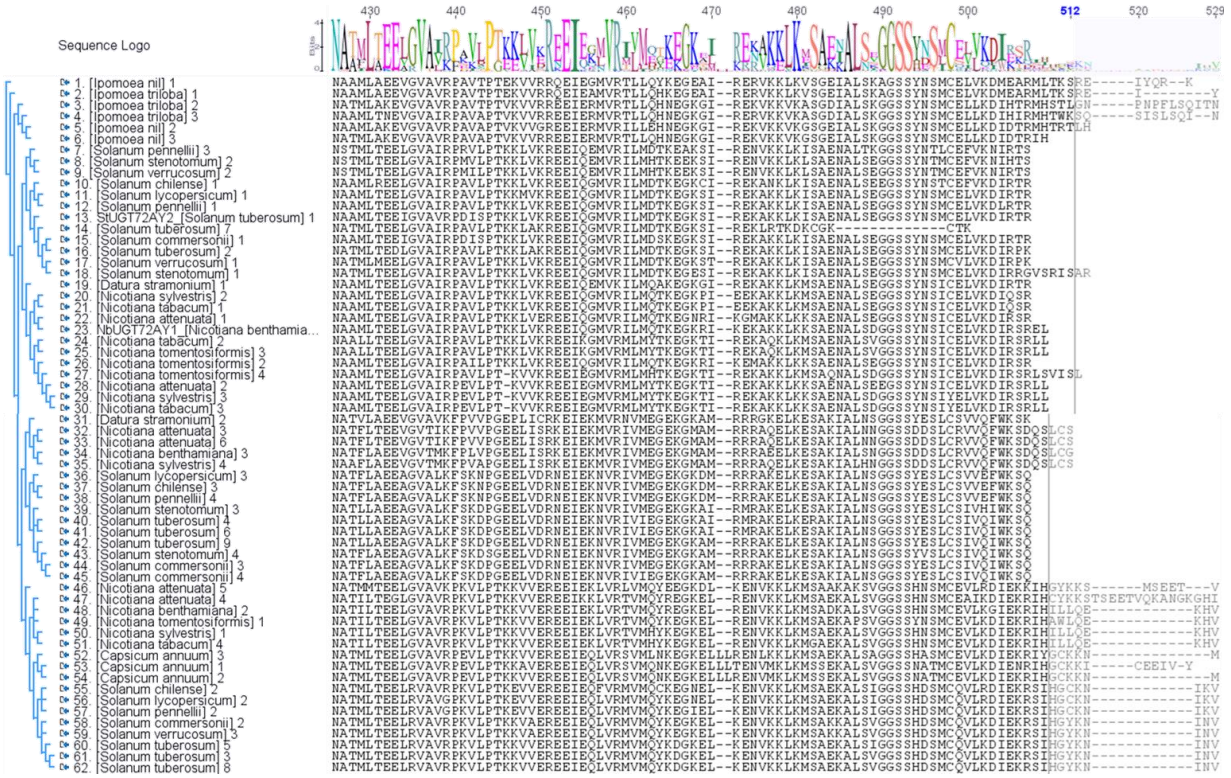

Fig. S19. Phylogenetic analysis of the closed homologues of NbUGT72AY1. The tree shows the protein sequences most similar to NbUGT72AY1 extracted from GenBank (www.ncbi.nlm.nih.gov/genbank/).

Part 3

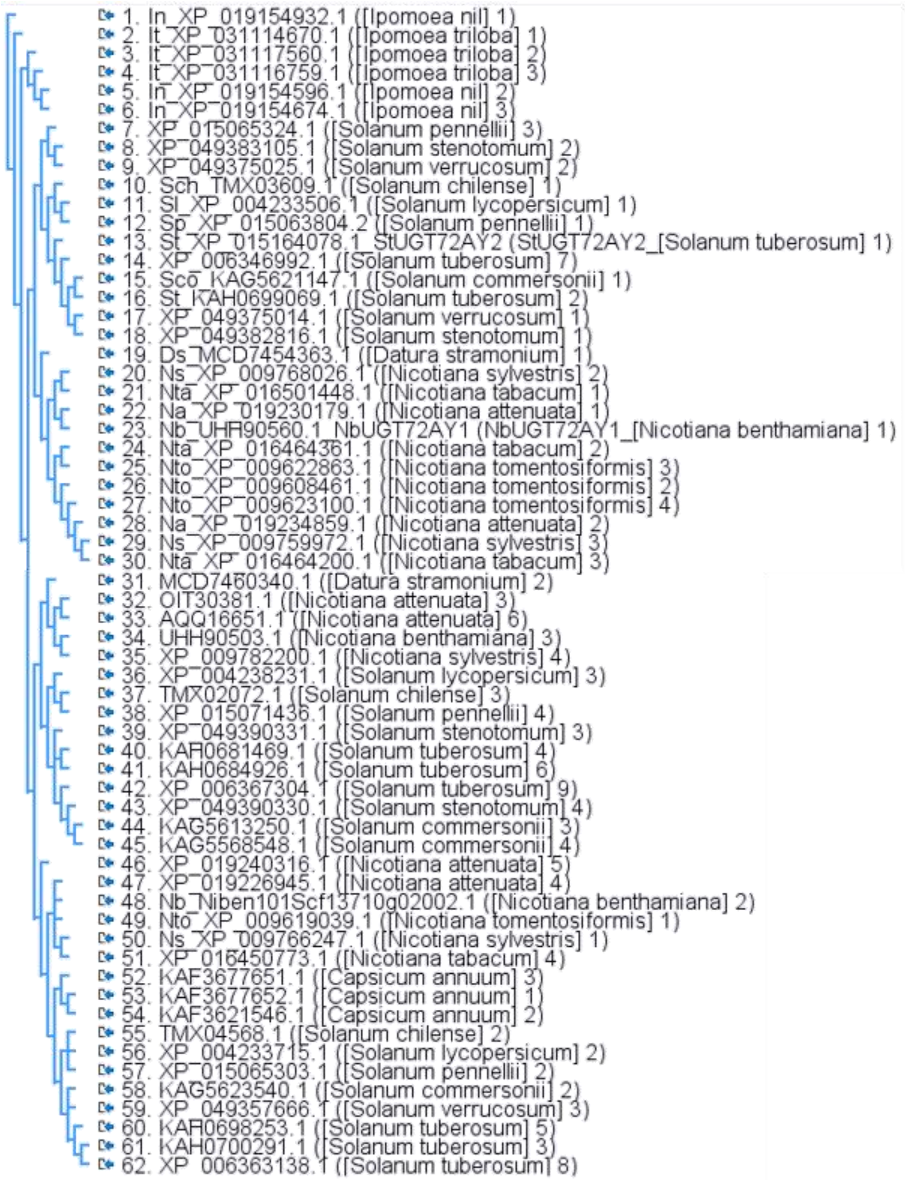

Fig. S20. Phylogenetic analysis of the closed homologues of NbUGT72AY1. The tree shows the accession numbers of the protein sequences most similar to NbUGT72AY1 extracted from GenBank (www.ncbi.nlm.nih.gov/genbank/).

Selected	Gene ID	Cluster	Most recent duplication	Similarity Score	Highest expressed tissue	Tissues specificity ▲	Sequence description	EC
☐	NIATv7_g08662	cluster000616	shared among Solanaceae	0.9907	leaf treated	0.9787	feruloyl ortho-hydroxylase 1-like	
☐	NIATv7_g21047	cluster013006	shared among *Nicotiana*	0.9828	leaf treated	0.9393	fruit-specific -like	
☐	NIATv7_g16562	cluster004316	shared among Solanaceae	0.9844	leaf treated	0.872	phosphoribulokinase, chloroplastic	2.7.1.48 2.7.1.19
☐	NIATv7_g30724	cluster001174	shared among *Nicotiana*	0.9566	leaf treated	0.8153	alpha-dioxygenase 1-like	1.11.1.7
☐	NIATv7_g16426	cluster001640	shared among *Nicotiana*	1	leaf treated	0.7788	anthocyanidin 3-O-glucosyltransferase 5-like	

Fig. S21. Co-expression analysis performed at http://nadh.ice.mpg.de/NaDH/network/gene_gene. The orthologue of NbUGT72AY1 from *N. attenuata* (XP_019230179) was used to screen for co-expressed genes in a *N. attenuate* transcriptome database.

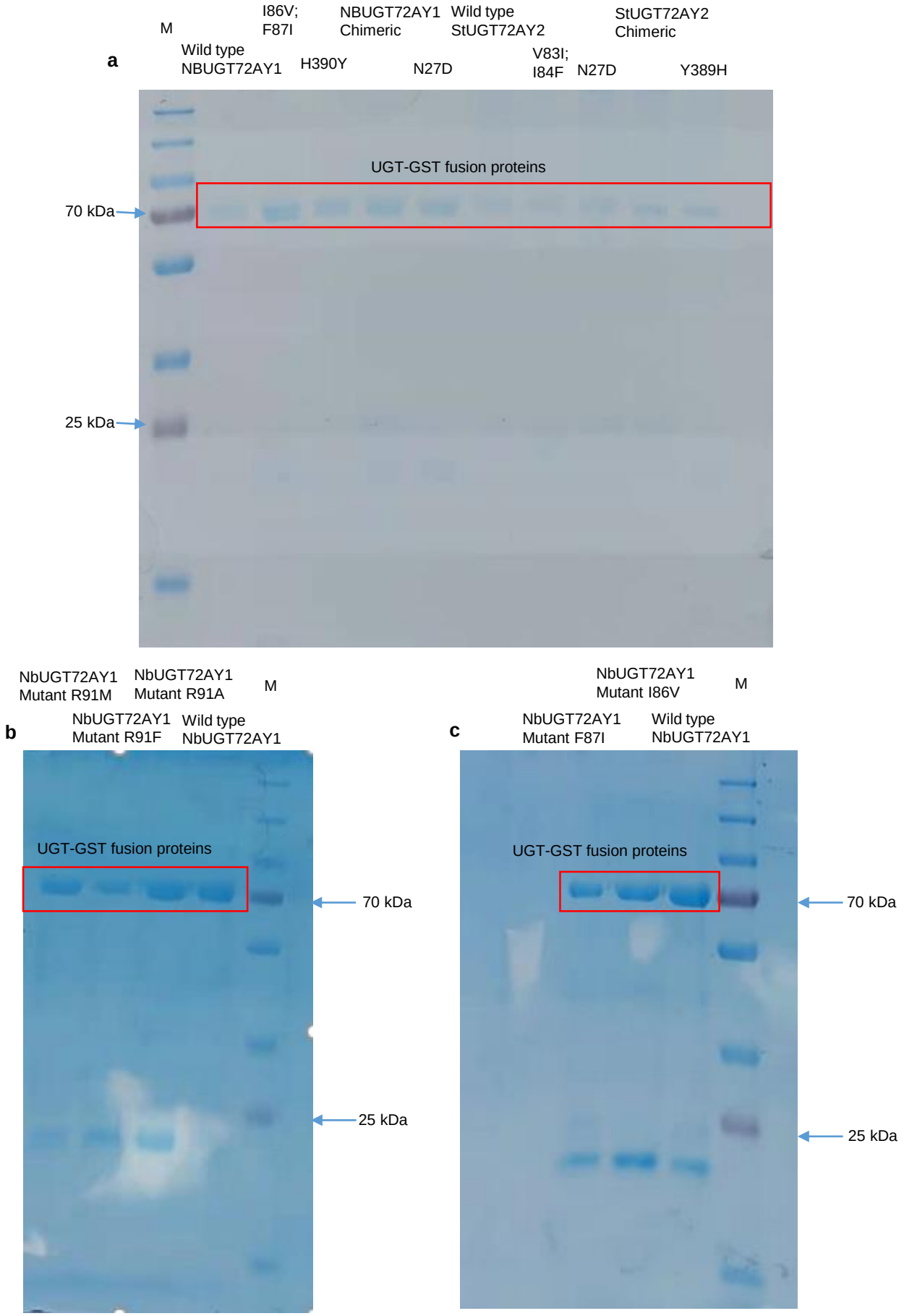

Fig. S22. SDS-PAGE analysis of NbUGT72AY1, StUGT72AY2 and their mutants. Gel was stained with Coomassie Blue. M: marker proteins (PageRuler Plus Prestained Protein Ladder marker). **a** Wild type NbUGT72AY1, NbUGT72AY1 Mutant I86V_F87I, NbUGT72AY1 Mutant H390Y, NbUGT72AY1 Mutant chimeric, NbUGT72AY1 Mutant N27D, Wild type StUGT72AY2, StUGT72AY2 Mutant V83I_I84F, StUGT72AY2 Mutant N27D, StUGT72AY2 Mutant chimeric, and StUGT72AY2 Mutant Y389H. **b** Wild type NbUGT72AY1, NbUGT72AY1 Mutant R91A, NbUGT72AY1 Mutant R91F, and NbUGT72AY1 Mutant R91M. **c** Wild type NbUGT72AY1, NbUGT72AY1 Mutant I86V, and NbUGT72AY1 Mutant F87I.

References

Brazier-Hicks, M., Offen, W.A., Gershater, M.C., Revett, T.J., Lim, E.K., Bowles, D.J., Davies, G.J., Edwards, R. (2007) Characterization and engineering of the bifunctional N- and O-glucosyltransferase involved in xenobiotic metabolism in plants. *Proc. Natl. Acad. Sci. U. S. A.* **104,** 20238-2043

He, J.B., Zhao, P., Hu, Z.M., Liu, S., Kuang, Y., Zhang, M., Li, B., Yun, C.H., Qiao, X., Ye, M. (2019) Molecular and structural characterization of a promiscuous C-glycosyltransferase from *Trollius chinensis*. Angew. *Chem. Int. Ed. Engl.* **58**, 11513-11520

Maharjan, R., Fukuda, Y., Shimomura, N., Nakayama, T., Okimoto, Y., Kawakami, K., Nakayama, T., Hamada, H., Inoue, T., Ozaki, S.I. (2020) An ambidextrous polyphenol glycosyltransferase PaGT2 from *Phytolacca americana*. *Biochemistry* **59**, 2551-2561

McGuffin, L.J., Adiyaman, R.; Maghrabi, A.H.A., Shuid, A.N.; Brackenridge, D.A., Nealon, J.O., Philomina, L.S. (2019) IntFOLD: an integrated web resource for high performance protein structure and function prediction. *Nucleic Acids Res.* **47**, W408-W413, doi:10.1093/nar/gkz322.

Shao, H., He, X., Achnine, L., Blount, J.W., Dixon, R.A., Wang, X. (2005) Crystal structures of a multifunctional triterpene/flavonoid glycosyltransferase from *Medicago truncatula*. *Plant Cell* **17**, 3141-3154

Waterhouse, A.; Bertoni, M.; Bienert, S.; Studer, G.; Tauriello, G.; Gumienny, R. et al. (2018): SWISS-MODEL: homology modelling of protein structures and complexes. *Nucleic acids research* **46** (W1), W296-W303. DOI: 10.1093/nar/gky427.